http://www.press.ierek.com

ISSN (Print: 2537-0731, online: 2537-074X)

Proceedings of Science and Technology

Research Paper

Received: 1 January 2024, Accepted: 14 July 2024, Published online: 30 September 2024

DOI: 10.21625/resourceedings.v4i2.1058

Effect of Nonlinear Magnetic Forces on Transverse Galloping Dynamics of Square Cylinders

Mostafa R. Rashed[1], Mostafa E.A. Elsayed[2], M.A. Abdelrahman[3], Mahmoud Shaaban[4,5]

[1]Assistant Professor, Mechanical Engineering Department, Faculty of Engineering, Modern University for Technology and Information, Cairo, Egypt

[2]Associate Professor, Automation and Energy Technology Lab, Mechanical Engineering Department, Faculty of Engineering at Shoubra, Benha University, Cairo, Egypt

[3]Associate Professor, Combustion and Energy Technology Lab, Mechanical Engineering Department, Faculty of Engineering at Shoubra, Benha University, Cairo, Egypt

[4]Assistant Professor, Mechanical Engineering Program, School of Engineering and Applied Sciences, Nile University, Giza, Egypt

[5] Assistant Professor, Smart Engineering Systems Center, Nile University, Giza, Egypt

Abstract

Under the influence of cross-fluid flow, a cylinder of a square cross-section may gallop. Galloping is a self-excited vibration mode that can be utilized for low-power harvesting applications. The harvested power depends on several factors, including upstream flow velocity and system dynamics. This study explores the potential of magnetically-induced nonlinear stiffness to improve the power output of galloping-based energy harvesters. In this experimental study, the vibration response of a square rod with a mass ratio of 10 is investigated at a Reynolds number of 200. The vibration behavior of two identical coaxial square rods with magnetic monopoles at opposite ends is analyzed. Results reveal that the magnets' configuration and strength significantly affect vibration amplitude and the critical flow velocity necessary for the onset of galloping.

Keywords

Galloping; Square cylinder; Energy harvesting; Nonlinear stiffness; CFD; Fluid-structure interaction; Vibration

1. Introduction

Flow-induced vibrations, including vortex-induced vibration, galloping, and flutter, can affect slender and flexible structures exposed to wind or water flows. These instabilities have been observed in a wide range of engineering structures, such as bridges (Zhang et al., 2020), tall buildings (Kawai, 1995), power transmission lines (Song et al., 2020), heat exchanger tubes (Paı¨doussis, 2006; Shaaban & Mohany, 2021), and ducts with cavities (Abdelmwgoud et al., 2021). The detrimental impact of these vibrations on structural fatigue life and safety is widely recognized (Song et al., 2021). On the positive side, there is an increasing focus on harnessing the energy from flow-induced vibrations as a sustainable and clean energy source (Lv et al., 2021; Ma & Zhou, 2022; Rostami & Armandei, 2017; Wang et al., 2020).

Galloping refers to a type of system instability characterized by significant oscillations in a structure when the speed of the incoming fluid increases. It occurs as a result of aeroelastic instability, wherein small oscillations initiate fluid

forces that gradually overpower the inherent damping of the structure. Notably, long and slender structures with non-circular cross-sections are susceptible to experiencing low-frequency, quasi-periodic motion when the flow velocity surpasses a certain threshold. If the fluid flows perpendicular to the structure's axis, it will gallop in the transverse direction. As the oscillations progress, the amplitude of displacement increases but eventually stabilizes due to a balance between the fluid damping forces and the reduced system damping, leading to the completion of a cycle.

Extensive research has been dedicated to understanding galloping in square-shaped structures (Mannini et al., 2014). Measurements by Nakamura and Mizota (Nakamura & Mizota, 1975) showed sudden changes in frequency and phase angles when critical flow velocities for vortex excitation and galloping were reached. Bearman and Obasaju (Bearman & Obasaju, 1982) found notable differences in force coefficients and phase characteristics between stationary square and circular cylinders. The behavior of the oscillating system is influenced by non-dimensional parameters, including the Reynolds number and reduced flow velocity. Transverse vibration response in square cylinders can be assessed using the root mean square displacement $y_{rms} = rms(Y)/L$ and the Strouhal number $St = fL/U$ (Shaaban & Mohany, 2022). Galloping amplitude increases almost linearly with reduced flow velocity Ur = U/(fnL) after surpassing a specific threshold. (Rashed et al., 2024) observed that nonlinear forces do not have a significant impact on the vibration frequency but can impact the vibration amplitude. Galloping initiation is typically associated with a minimum displaced mass ratio $m^* = m/\rho L^2$, and the onset Reynolds number weakly depends on the mass ratio (Sen & Mittal, 2011, 2016).

Accurately modeling and predicting the performance of vibrating energy harvesters with nonlinear forces is a persistent challenge (Ma & Zhou, 2022). Nonlinear devices often face chaos and bifurcation, necessitating an exploration of the impact of nonlinearity on performance and stability (Huynh & Tjahjowidodo, 2017). (Shaaban & Mohany, 2021) successfully used coupled modeling to predict forces exerted by airflow due to vortex shedding. Existing literature suggests that nonlinear forces generally improve power output and stability in energy harvesters, but the underlying mechanisms and effects require further investigation. Understanding the influence of nonlinear forces on galloping energy harvesters can facilitate amplitude control and suppression in unfavorable vibration conditions.

This study aims to examine the influence of a nonlinear magnetic force on the performance of a galloping energy harvester. To investigate the dynamic behavior, a numerical flow simulation based on the incompressible Navier-Stokes equation, coupled with a double-structure single-degree-of-freedom solver, is employed. The harvester design consists of two galloping objects coupled through a magnetic repulsion force. A configuration of the nonlinear magnetic monopoles is explored. The strength of the magnetic field and repulsion force is varied to assess its impact on the galloping response and dynamic stability of the system.

2. Methodology

2.1. Numerical Model

Figure 1 displays a schematic of the configuration under investigation. It consists of two identical rods attached to springs, allowing movement in the transverse direction only. The rods are separated by a distance equal to their edge length. For the reference case without magnetic forces, the rods have a mass ratio $m^* = 10$ ensuring a typical galloping response. The flow is laminar at a constant Reynolds number $Re = 200$, eliminating turbulence's influence and facilitating comparison with other studies (Joly et al., 2012). The system's natural frequency is controlled by varying the structural stiffness, while two magnetic poles at the ends produce repulsive forces as the rods oscillate.

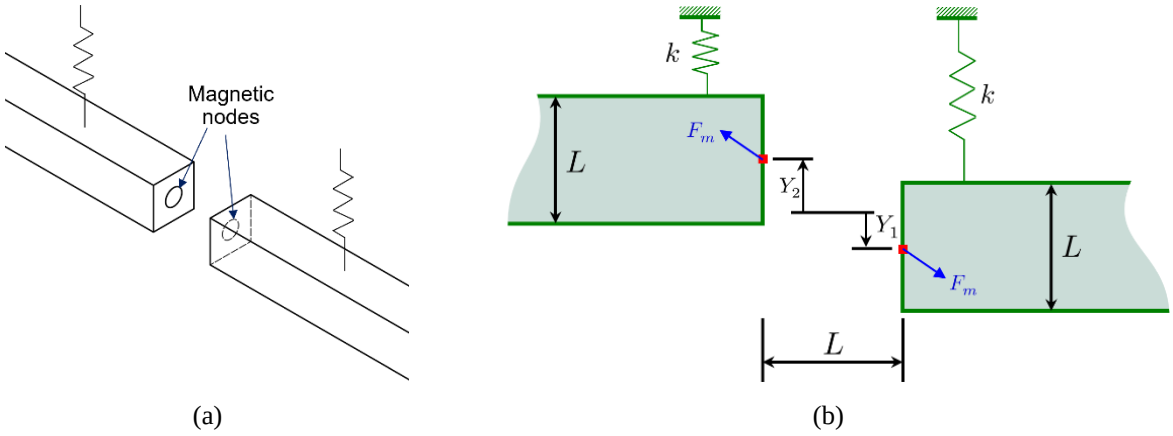

Figure 1: (a) A schematic of the investigated configuration and (b) the parameters of the investigated configuration.

Figure 2 displays the computational domain used in the simulation, with the same extensions used by Li et al. (Li et al., 2019) in the upstream, downstream, and width directions. Two quadrilateral grid zones, each with 85,000 elements, were employed to calculate the flow around the square cross sections independently. Flow field calculations are updated in both zones to accurately determine the phase between their motion, which is influenced solely by the transverse component of the repulsive magnetic force. The grid is orthogonal, and the square walls are resolved by 200 elements. Boundary conditions from Figure 2 are applied to both zones, with varying values for the location and velocity of the square cross-section wall based on the previous time step. Inlet and side conditions include a fixed flow velocity and zero pressure gradient. The outlet condition specifies a reference pressure that doesn't affect the incompressible solution. The square section walls have a no-slip condition. Pressure-velocity coupling employs a pressure implicit scheme with operator splitting. Second-order upwind discretization is used for convective terms, while a least-squares scheme calculates gradients. Time derivatives are resolved using a bounded second-order scheme.

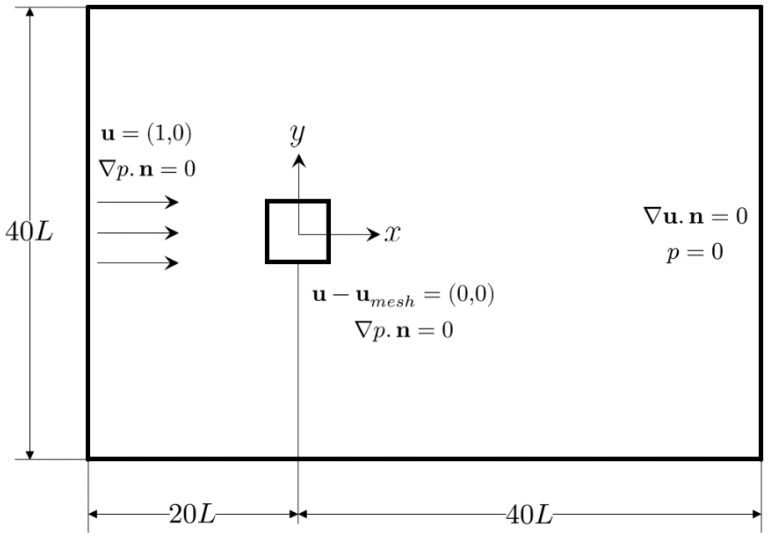

Figure 2: The utilized computational domain and the boundary conditions.

2.2. Governing Equations

The transverse displacement Y of a two-dimensional square cylinder, which is supported elastically and exposed to both flow and magnetic forces, can be described by a straightforward oscillator equation. The equation considers parameters such as mass m, damping c, stiffness k, and the influence of pressure P on displacement.

$$m\ddot{Y} + c\cdot\dot{Y} + kY = \left(\int P d\mathbf{A} + \mathbf{F}_m\right)\cdot \mathbf{j} \quad (1)$$

The transient incompressible Navier-Stokes equations are solved to obtain the flow field and calculate the overall fluid pressure force acting on the cylinders.

$$\nabla \cdot \mathbf{u}_l = 0, \tag{2}$$

$$\frac{\partial \mathbf{u}_l}{\partial t} = -\left(\mathbf{u}_l \cdot \nabla\right)\mathbf{u}_l - \nabla p + \frac{1}{Re}\nabla^2 \mathbf{u}_l, \tag{3}$$

where the Lagrangian flow velocity $\mathbf{u}_l = \mathbf{u} - \mathbf{u}_{mesh}$. The absolute velocity vector $\mathbf{u}$ is normalized by the upstream flow velocity U . The mesh velocity $\mathbf{u}_{mesh}$ is determined based on the velocity of the solid structure's boundary, computed using equation (1). $p = P/\rho U^2$ is the normalized pressure. The Reynolds number in a fluid of viscosity μ is $Re = \rho U_\infty D/\mu$. The formulation for body forces in the flow and structure domains does not incorporate gravity. The cylinder edge length L serves as the reference length scale, while the upstream flow velocity acts as the reference flow velocity U.

On the other hand, the magnetic repulsion force is determined by considering a simplified configuration that represents the ideal scenario of a pair of monopoles with the same charge sign. The repulsion force between two monopoles of equal strength q can be calculated as follows:

$$\mathbf{F}_m = q\mathbf{B} = \frac{q^2}{4\pi\mu_0 r^2}\hat{\mathbf{r}}, \tag{4}$$

where $\hat{\mathbf{r}}$ is the direction vector between the two poles, $r = \sqrt{L^2 - (Y_2 - Y_1)^2}$ is its magnitude and μ_0 is the permeability. Setting $C_b = q^2/4\pi\mu_0 L^3$ as a constant that represents the relative strength of the pole pair, the cross-flow force component is dependent on the location of the two squares. Equation 5 shows that the force induced by the monopoles is a nonlinear stiffness force.

$$F_{m_Y} = \mathbf{F}_m \cdot \mathbf{j} = C_B \frac{Y_2 - Y_1}{\left[1 + \left(\frac{Y_2 - Y_1}{L}\right)^2\right]^{3/2}} \tag{5}$$

The solver inputs the previous flow field data and cross-section locations/velocities. An iterative flow solver (outlined in Figure 3) determines the pressure field and provides updated flow data. Using their locations, the structural solver calculates the transverse magnetic forces on the cross-sections. It then updates their velocity and location. This process repeats until a steady oscillating behavior is achieved, allowing spectral domain calculations.

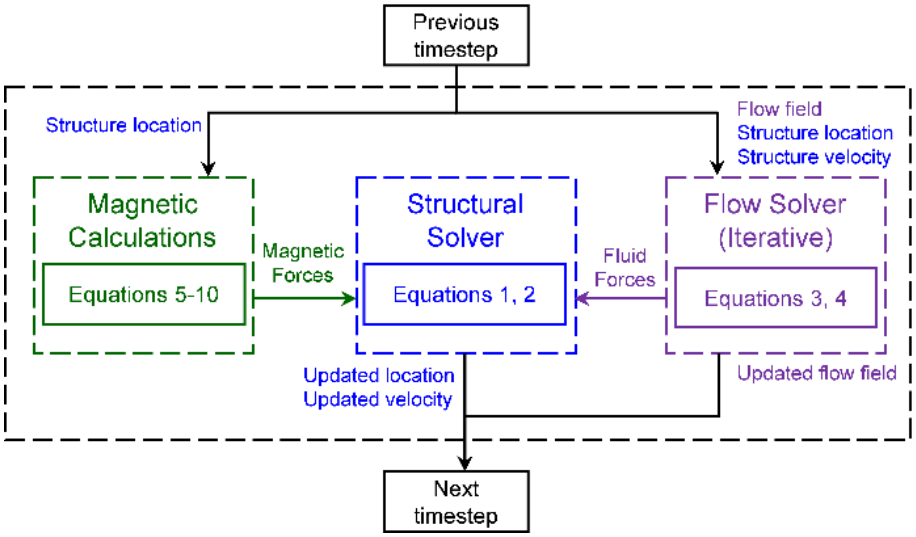

Figure 3: The solver algorithm.

2.3. Model Validation

In order to ensure the computational model reliability, a grid sensitivity analysis was conducted employing three grid configurations G1, G2, and G3, listed in Table 1. The study showed that the grid configuration G2 provided satisfactory results.

Table 1: Grid sensitivity analysis for a stationary square cylinder at $Re = 200$.

Grid	Number of Elements	C_d
G1	27,500	1.53
G2	85,000	1.47
G3	192,000	1.46

The numerical model's results are compared and validated against existing data for square cylinders carried out by Li et al. (Li et al., 2019) at Reynolds number $Re = 150$.

Figure 4 demonstrates that the numerical model employed during the present study effectively captures the oscillation amplitude and critical flow velocity for all flow-induced vibration mechanisms.

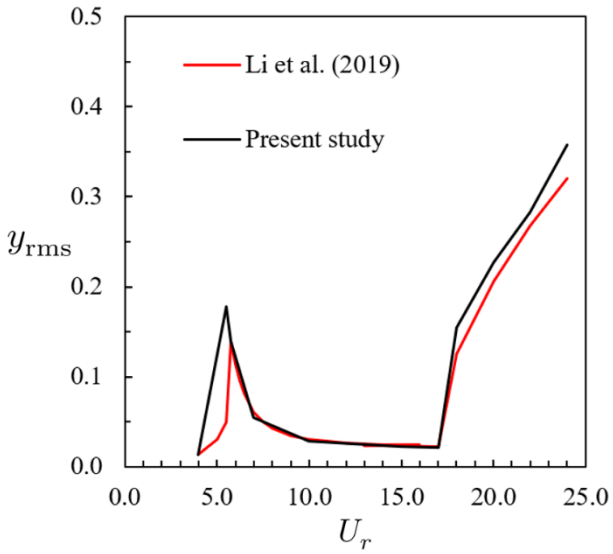

Figure 4: The galloping response of a square rod cylinder at $Re = 150$, compared with the results of (Li et al., 2019).

3. Results and Discussions

In this section, the galloping response of the two bluff bodies with square cross sections is analyzed to determine the influence of the nonlinear stiffness added by the magnetic repulsion force. As seen in Figure 5, the effect of the reduced velocity on the galloping response of the bluff bodies is dependent on the strength factor C_B, correlated to the relative strength of the nonlinear stiffness to the linear spring stiffness. The impact of reduced flow velocity on the flow-induced vibration response is shown for the three considered cases: a linear spring system, a system with a pair of weak magnetic monopoles, and a system with a pair of stronger magnetic monopoles.

For the linear spring case $C_B = 0$, vortex-induced vibration results in significant vibration amplitude reaching up to $y_{rms} = 0.25$, while the galloping response starts after the flow velocity exceeds $U_r = 10$. As the flow velocity increases beyond that limit, the amplitude of vibration increases, reaching twice the vortex-induced value at $U_r = 20$. The influence of non-linear stiffness can be observed in Figure 5. For the vortex-induced vibration, the repulsion force induced by the magnetic monopoles resulted in a decrease in amplitude at $U_r = 5$. It is, however, unclear if the amplitude decreased as the resonance frequency shifted to a slightly different value, or if the stiffness change resulted in an overall decrease in the vibration amplitude for vortex-induced vibration. On the other hand, the nonlinear

repulsion forces caused by magnetic monopoles resulted in two effects in the galloping flow velocity range. First, an enhancement of the galloping amplitude is observed such that at $U_r = 20$, the amplitude reaches $y_{rms} = 0.55$, and $y_{rms} = 0.8$ for $C_B = 0.1$ and $C_B = 1.0$; respectively, increasing from 0.5 for the linear system. This enhancement can be attributed to the linear contribution of the stiffness increased by the magnetic force at positions close to the original mass location.

The second effect of the nonlinear stiffness is a decrease in the onset velocity required for galloping. The reduced flow velocity at the onset of galloping decreased from $U_r = 10$ for the linear system, to about $U_r = 8$ for $C_B = 1.0$. This decrease is attributed to the overall decrease of stiffness caused by the nonlinear force, which results in the galloping range shift to lower reduced velocities, which is equivalent to a reduction in wind speed requirements for galloping energy harvesting.

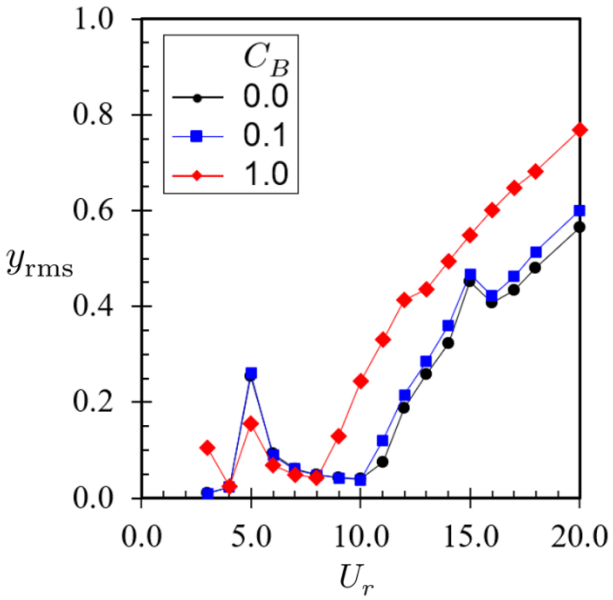

Figure 5: Impact of reduced velocity U_r on the response of flow-induced vibration characteristics under various levels of repulsive force strength.

Figure 6 compares the vibration-time signal of the two structures under the presence of magnetic monopoles with different strengths before and after the onset of galloping, as illustrated in Figure 5). Under galloping conditions, magnetic monopoles with a strength of $C_B = 0.1$ result in slightly higher motion amplitude than in situations without repulsive forces. This effect becomes more noticeable when monopoles of higher strength, $C_B = 1.0$, are introduced, leading to a significant increase in the root mean square of motion, particularly at $U_r = 12$. In addition, Figure 6 shows the signal characteristics in the time domain, revealing that while the amplitude of the motion is the same for the two objects in all cases, the relative phase between them is affected by the strength of the magnetic repulsion force. As expected, the linear system has the two objects moving at an arbitrary phase as no coupling between them is present. In contrast, the two cases with a magnetic repulsion force exhibit a phase of 180°, indicating an out-of-phase behavior. This is to be expected, as this phase results in oscillation between the highest and the least potential energy states in the magnetic field. As such, this coupling can be used to control the behavior of the bluff bodies and tie their timing which may be beneficial to their mechanical characteristics in devices designed for energy harvesting from fluid flow.

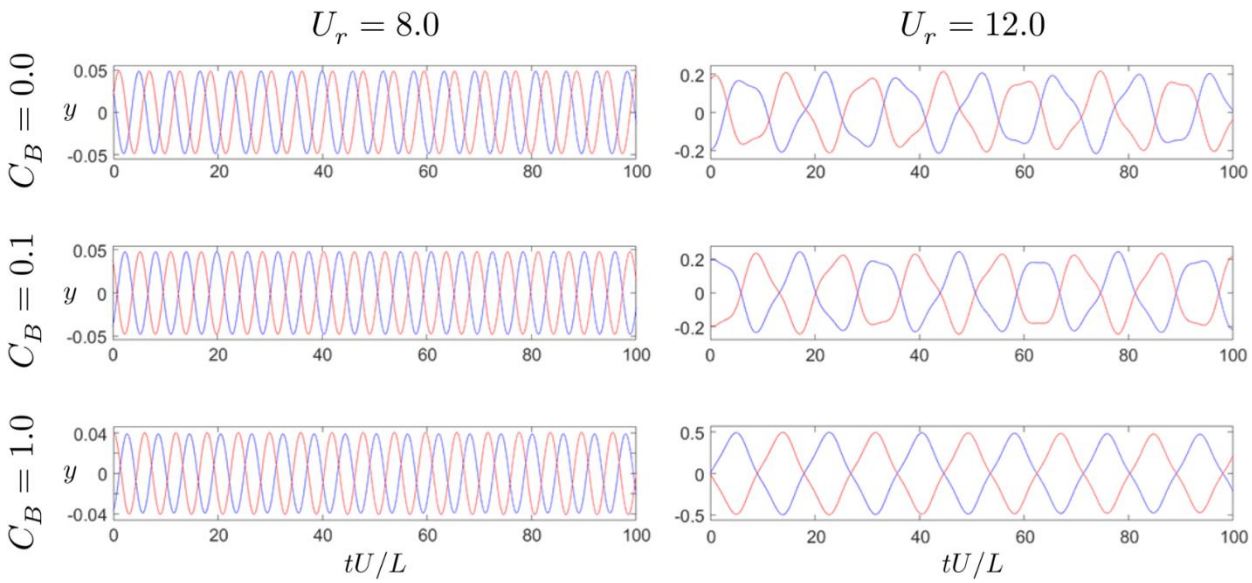

Figure 6: Vibration-time signal comparison of the two structures with and without nonlinear monopole magnetic effect.

4. Conclusions

The galloping response of a bluff body with a square cross-section depends on the stiffness characteristics of the system. In this study, the impact of a nonlinear magnetically-induced force on the vibration response of two coaxial rods with square cross-sections and identical structural parameters is numerically investigated. To calculate the galloping response of two bluff bodies interacting through a magnetic repulsion force, a fully-coupled finite element model is used to calculate the forces affecting the two bodies from effects including fluid flow, magnetic repulsion, and structural forces. The galloping response is investigated at $Re = 200$ and $m^* = 10$ for a linear system and compared with the case of two levels of magnetic field strength.

Results showed that a nonlinear repulsion force between magnetic monopoles enhances vibration amplitude and reduces onset flow velocity requirements. Evidently, the increase in vibration amplitude is attributed to a substantial negative stiffness generated by the magnets' repulsion. On the other hand, the magnetic force strength has a minimal impact on galloping vibration frequency, which is primarily determined by amplitude. This vibration amplitude enhancement is significant for powerful magnetic forces and can potentially enhance the performance of galloping-based flow energy harvesting devices. In addition, the magnetic repulsion force results in a coupling such that the phase between the motion of the two objects is $180°$ out of phase.

Acknowledgment

The abstract of this paper was presented at the Environmental Design, Material Science, and Engineering Technologies (EDMSET) Conference – 1st Edition which was held on the 22nd-24th of April 2024.

Funding declaration

This research did not receive any specific grant from funding agencies in the public, commercial, or not-for-profit sectors/individuals.

Ethics approval

Not applicable.

Conflict of interest

The authors declare that there is no competing interest.

References

Abdelmwgoud, M., Shaaban, M., & Mohany, A. (2021). Shear layer synchronization of aerodynamically isolated opposite cavities due to acoustic resonance excitation. *Physics of Fluids*, *33*(5). https://doi.org/10.1063/5.0051226

Bearman, P. W., & Obasaju, E. D. (1982). An experimental study of pressure fluctuations on fixed and oscillating square-section cylinders. *Journal of Fluid Mechanics*, *119*, 297–321. https://doi.org/10.1017/S0022112082001360

Huynh, B. H., & Tjahjowidodo, T. (2017). Experimental chaotic quantification in bistable vortex induced vibration systems. *Mechanical Systems and Signal Processing*, *85*, 1005–1019. https://doi.org/10.1016/j.ymssp.2016.09.025

Joly, A., Etienne, S., & Pelletier, D. (2012). Galloping of square cylinders in cross-flow at low Reynolds numbers. *Journal of Fluids and Structures*, *28*, 232–243. https://doi.org/10.1016/j.jfluidstructs.2011.12.004

Kawai, H. (1995). Effects of angle of attack on vortex induced vibration and galloping of tall buildings in smooth and turbulent boundary layer flows. *Journal of Wind Engineering and Industrial Aerodynamics*, *54–55*, 125–132. https://doi.org/10.1016/0167-6105(94)00035-C

Li, X., Lyu, Z., Kou, J., & Zhang, W. (2019). Mode competition in galloping of a square cylinder at low Reynolds number. *Journal of Fluid Mechanics*, *867*, 516–555. https://doi.org/10.1017/jfm.2019.160

Lv, Y., Sun, L., Bernitsas, M. M., & Sun, H. (2021). A comprehensive review of nonlinear oscillators in hydrokinetic energy harnessing using flow-induced vibrations. *Renewable and Sustainable Energy Reviews*, *150*, 111388. https://doi.org/10.1016/j.rser.2021.111388

Ma, X., & Zhou, S. (2022). A review of flow-induced vibration energy harvesters. *Energy Conversion and Management*, *254*, 115223. https://doi.org/10.1016/j.enconman.2022.115223

Mannini, C., Marra, A. M., & Bartoli, G. (2014). VIV–galloping instability of rectangular cylinders: Review and new experiments. *Journal of Wind Engineering and Industrial Aerodynamics*, *132*, 109–124. https://doi.org/10.1016/j.jweia.2014.06.021

Nakamura, Y., & Mizota, T. (1975). Unsteady Lifts and Wakes of Oscillating Rectangular Prisms. *Journal of the Engineering Mechanics Division*, *101*(6), 855–871. https://doi.org/10.1061/JMCEA3.0002077

Paı¨doussis, M. P. (2006). Real-life experiences with flow-induced vibration. *Journal of Fluids and Structures*, *22*(6–7), 741–755. https://doi.org/10.1016/j.jfluidstructs.2006.04.002

Rashed, M. R., Elsayed, M. E. A., & Shaaban, M. (2024). Influence of magnetically-induced nonlinear added stiffness on the lift galloping of square cylinders at low Reynolds number. *Journal of Fluids and Structures*, *124*, 104046. https://doi.org/10.1016/j.jfluidstructs.2023.104046

Rostami, A. B., & Armandei, M. (2017). Renewable energy harvesting by vortex-induced motions: Review and benchmarking of technologies. *Renewable and Sustainable Energy Reviews*, *70*, 193–214. https://doi.org/10.1016/j.rser.2016.11.202

Sen, S., & Mittal, S. (2011). Free vibration of a square cylinder at low Reynolds numbers. *Journal of Fluids and Structures*, *27*(5–6), 875–884. https://doi.org/10.1016/j.jfluidstructs.2011.03.006

Sen, S., & Mittal, S. (2016). Free Vibrations of a Square Cylinder of Varying Mass Ratios. *Procedia Engineering*, *144*, 34–42. https://doi.org/10.1016/j.proeng.2016.05.004

Shaaban, M., & Mohany, A. (2021). Synchronous vortex shedding from aerodynamically isolated side-by-side cylinders imposed by flow-excited resonant acoustic modes. *Experiments in Fluids*, *62*(10), 205. https://doi.org/10.1007/s00348-021-03301-9

Shaaban, M., & Mohany, A. (2022). Flow–acoustic coupling around rectangular rods of different aspect ratios and incidence angles. *Experiments in Fluids*, *63*(2), 45. https://doi.org/10.1007/s00348-022-03380-2

Song, Y., Liu, Z., Rxnnquist, A., Navik, P., & Liu, Z. (2020). Contact Wire Irregularity Stochastics and Effect on High-speed Railway Pantograph-Catenary Interactions. *IEEE Transactions on Instrumentation and Measurement*, 1–1. https://doi.org/10.1109/TIM.2020.2987457

Song, Y., Wang, Z., Liu, Z., & Wang, R. (2021). A spatial coupling model to study dynamic performance of pantograph-catenary with vehicle-track excitation. *Mechanical Systems and Signal Processing*, *151*, 107336. https://doi.org/10.1016/j.ymssp.2020.107336

Wang, J., Geng, L., Ding, L., Zhu, H., & Yurchenko, D. (2020). The state-of-the-art review on energy harvesting from flow-induced vibrations. *Applied Energy*, *267*, 114902. https://doi.org/10.1016/j.apenergy.2020.114902

Zhang, M., Xu, F., & Han, Y. (2020). Assessment of wind-induced nonlinear post-critical performance of bridge decks. *Journal of Wind Engineering and Industrial Aerodynamics*, *203*, 104251. https://doi.org/10.1016/j.jweia.2020.104251